

PAPER • OPEN ACCESS

## Double-propagation mode in short-gap spark discharges driven by HV pulses with sub-ns rise time

To cite this article: H Höft *et al* 2020 *Plasma Sources Sci. Technol.* **29** 085002

View the [article online](#) for updates and enhancements.

You may also like

- [Erratum: Noise-induced transition in human reaction times \(2016 \*J. Stat. Mech.: Theory Exp.\* \*\*9\*\* 093502\)](#)  
José M Medina and José A Díaz
- [Tractable calculation of the Green's tensor for shear wave propagation in an incompressible, transversely isotropic material](#)  
Ned C Rouze, Mark L Palmeri and Kathryn R Nightingale
- [Tool changing 3D printer for rapid prototyping of advanced soft robotic elements](#)  
Stefan Conrad, Thomas Speck and Falk J Tauber

Recent citations

- [Generation of runaway electrons in plasma after a breakdown of a gap with a sharply non-uniform electric field strength distribution](#)  
D V Beloplotov *et al*



# Instruments for Advanced Science

- Knowledge,
- Experience,
- Expertise

[Click to view our product catalogue](#)

Contact Hiden Analytical for further details:  
[www.HidenAnalytical.com](http://www.HidenAnalytical.com)  
[info@hiden.co.uk](mailto:info@hiden.co.uk)

Gas Analysis	Surface Science	Plasma Diagnostics	Vacuum Analysis
 <ul style="list-style-type: none"><li>dynamic measurement of reaction gas streams</li><li>catalysis and thermal analysis</li><li>molecular beam studies</li><li>dissolved species probes</li><li>fermentation, environmental and ecological studies</li></ul>	 <ul style="list-style-type: none"><li>UHV-TPD</li><li>SIMS</li><li>end point detection in ion beam etch</li><li>elemental imaging - surface mapping</li></ul>	 <ul style="list-style-type: none"><li>plasma source characterization</li><li>etch and deposition process reaction kinetic studies</li><li>analysis of neutral and radical species</li></ul>	 <ul style="list-style-type: none"><li>partial pressure measurement and control of process gases</li><li>reactive sputter process control</li><li>vacuum diagnostics</li><li>vacuum coating process monitoring</li></ul>

# Double-propagation mode in short-gap spark discharges driven by HV pulses with sub-ns rise time

H Höft<sup>1,4</sup> , M M Becker<sup>1</sup> , J F Kolb<sup>1,2</sup>  and T Huiskamp<sup>3</sup> 

<sup>1</sup> Leibniz Institute for Plasma Science and Technology (INP Greifswald), Felix-Hausdorff-Str. 2, 17489 Greifswald, Germany

<sup>2</sup> Institute of Physics, University of Rostock, Albert-Einstein-Str. 23–24, 18059 Rostock, Germany

<sup>3</sup> Dept. of Electr. Engineering, Eindhoven University of Technology, P.O. Box 513, 5600 MB Eindhoven, The Netherlands

E-mail: [hans.hoeft@inp-greifswald.de](mailto:hans.hoeft@inp-greifswald.de)

Received 27 February 2020, revised 29 May 2020

Accepted for publication 29 June 2020

Published 4 August 2020



CrossMark

## Abstract

The object of this study is the investigation of spark discharges ignited by unipolar positive rectangular high voltage (HV) pulses with 200 ps rise time and  $(15 \pm 2)$  kV amplitude with 3 ns duration full width at half maximum in synthetic air in a 1.2 mm pin-to-pin gap (tungsten electrodes) at atmospheric pressure. The discharge development was recorded by synchronised iCCD and streak camera measurements in single-shot operation, revealing a two-stage propagation mode. The discharge started with a fast initial breakdown across the entire gap ( $\sim 10 \text{ mm ns}^{-1}$ ) during the HV slope, followed by a much slower ( $\sim 0.1 \text{ mm ns}^{-1}$ ) propagation originating from both electrodes towards the gap centre. The combination of high-resolution diagnostics with numerical modelling indicated that the initial breakdown phase is caused by the rapid increase of electric field strength during the steep HV slope, which leads to the simultaneous fast propagation of a positive and a negative streamer.

Keywords: sub-ns breakdown, spark discharge, 2D fluid modelling, fast optical diagnostics, double streamer propagation

(Some figures may appear in colour only in the online journal)

## 1. Introduction

The breakdown of pulsed discharges at elevated pressures is a crucial topic in current research on the subject of non-thermal plasmas, because some fundamental open questions still remain, particularly concerning the discharge inception for steep high voltage (HV) slopes [1–3]. Since they can efficiently generate reactive species, these kind of discharges are very promising for various applications, such as air pollution control [4]. The slope steepness and the width of the HV

pulses driving the discharges are important parameters influencing the breakdown mechanisms and efficiency of reactive species production [5–9]. Numerous experiments have investigated the breakdown process under fast HV pulses with  $\sim 1$  ns rise time in cm-scale pin-to-plate arrangements, where the steep HV slope leads to relatively large discharge diameters of several mm during the initial discharge phase, e.g. in [3, 10, 11]. These mm-wide streamers have also been reproduced by numerical modelling for sub-ns rise times [12]. The formation of these wide diffuse discharges has been related to runaway electrons [13, 14], which play an important role for fast pulsed discharges, especially in longer gaps with very HV amplitudes. Pulsed discharges in shorter gaps of a few mm have mainly been investigated for the purposes of plasma-assisted combustion [2, 15]. An overview of different discharge

<sup>4</sup> Author to whom any correspondence should be addressed.



Original content from this work may be used under the terms of the [Creative Commons Attribution 4.0 licence](https://creativecommons.org/licenses/by/4.0/). Any further distribution of this work must maintain attribution to the author(s) and the title of the work, journal citation and DOI.

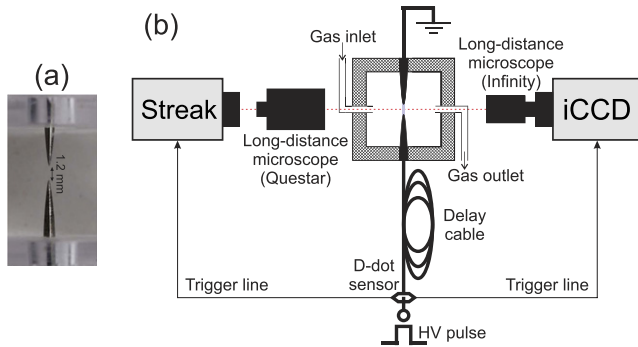


**Figure 1.** Photograph of pin-to-pin electrode configuration (a), and schematic representation of the experimental set-up, including diagnostics (b). See figure 3 for details of the actual HV connection to the cell.

regimes, including corona, glow, and spark discharges produced by nanosecond repetitive HV pulses in pin–pin configuration is given in [16].

The aim of the present study is to examine the discharge inception in a mm-sized pin-to-pin gap in atmospheric pressure air using a rectangular HV pulse with sub-ns rise time under overvoltage condition, i.e. using much higher HV amplitudes than the static breakdown/inception voltage. These voltages are required to ensure the ignition of the discharge during the HV slope without inception time lags [1]. Due to the very short voltage rise time, the electric field strength in the gap rises at the same time scale required by a streamer to propagate over 1 mm [8, 17, 18], or even faster. Consequently, the occurrence of a fast breakdown is expected, which differs from the streamer breakdown mechanism usually observed under unipolar positive HV pulses [16].

## 2. Experimental set-up and HV pulse source

For the purposes of the current study, a symmetrical pin-to-pin arrangement with a 1.2 mm gap (see figure 1(a)) was constructed using tungsten electrodes with  $\approx 25 \mu\text{m}$  tip radius. These electrodes were mounted in a Plexiglass cell (using the same cell geometry as detailed in [19]), flushed with dry synthetic air (Linde, purity 5.5) at a 500 sccm total gas flow rate. The breakdown and development of the discharges were tracked by synchronised iCCD and streak camera recordings (both spectrally integrated), which were simultaneously triggered by the applied HV pulse itself (see figure 1(b)). The iCCD camera (Stanford 4 Picos, temporal resolution  $\Delta t \geq 200 \text{ ps}$ ) was connected to a long-distance microscope (Infinity KX InfiniMax with MX-5 objective) providing a spatial resolution ( $\Delta x$ ) of  $13 \mu\text{m}$ . The streak camera system (HAMAMATSU C5680,  $\Delta t \geq 5 \text{ ps}$ ) recorded the discharge from the opposite side using a Questar QM100 long-distance microscope ( $\Delta x = 2 \mu\text{m}$ ). A temporal jitter correction was subsequently applied to overcome the 50 ps trigger jitter. In this way, synchronised iCCD and streak images of the same discharge event were obtained.

The discharge was operated by rectangular, unipolar positive HV pulses (with the system described in [21]) with a

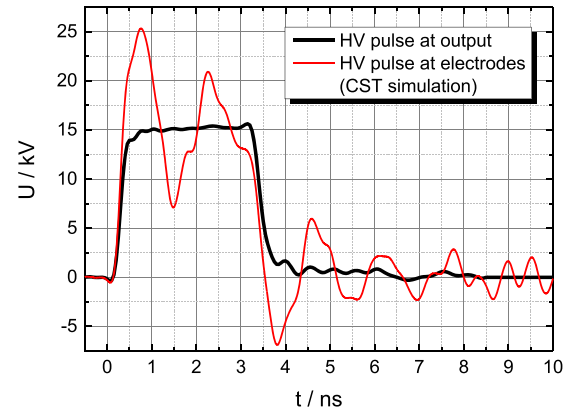


**Figure 2.** Applied HV pulse with 200 ps rise time and 3 ns FWHM duration at the pulse generator output, and the simulated HV waveform at the powered electrode. This simulated waveform was obtained using CST Studio Suite®, and it is important to note that this simulation was performed without a conducting channel.

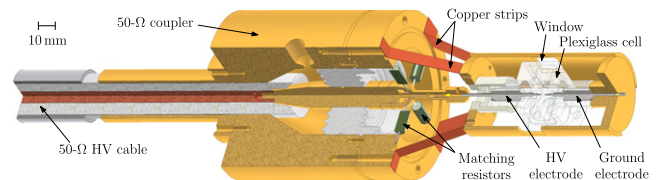


**Figure 3.** Three-quarter section view of the discharge arrangement connected to the 50- $\Omega$  HV cable of the pulse source. The cable is first connected to a cable coupler (explained in more detail in [20]), maintaining the 50- $\Omega$  impedance. This coupler was connected to the discharge arrangement with copper strips, and the cable coupler was terminated with matching resistors so as to avoid pulse reflections in the system as much as possible.

200 ps rise time and a 3 ns duration (full width at half maximum (FWHM)) at a pulse repetition frequency of 1 Hz, in order to avoid any influence of pre-ionisation on the subsequent discharge event. The characteristic voltage waveform at the output of the pulse source (black line), which was measured with a D-dot sensor [22], is shown in figure 2. The actual connection of the discharge arrangement to the pulse source is sketched in figure 3.

Due to the stochastic nature of the spark gap switching voltage within the pulse source (see figure 19 in [23]), the amplitude of the HV output pulse is  $(15 \pm 2) \text{ kV}$ . In addition, the actual voltage applied at the powered electrode is distorted, since the discharge arrangement is not impedance-matched to the 50- $\Omega$  HV cable. To improve this matching and to avoid reflections of the HV pulses between the discharge cell and the pulse source as much as possible, resistors were placed in parallel to the discharge cell, so as to approximate the 50- $\Omega$  impedance of the cable more closely (see figure 3 for more details). Measuring the HV waveform over the small electrodes is not straightforward (e.g. due to its sub-ns rise time), and was not attempted at this time, but saved for future experiments. Instead, the resulting HV waveform at the electrodes was obtained via 3D transient EM simulations with CST Studio Suite®, as displayed in figure 2. Here, it is important to note that while the actual geometry of the setup was taken into

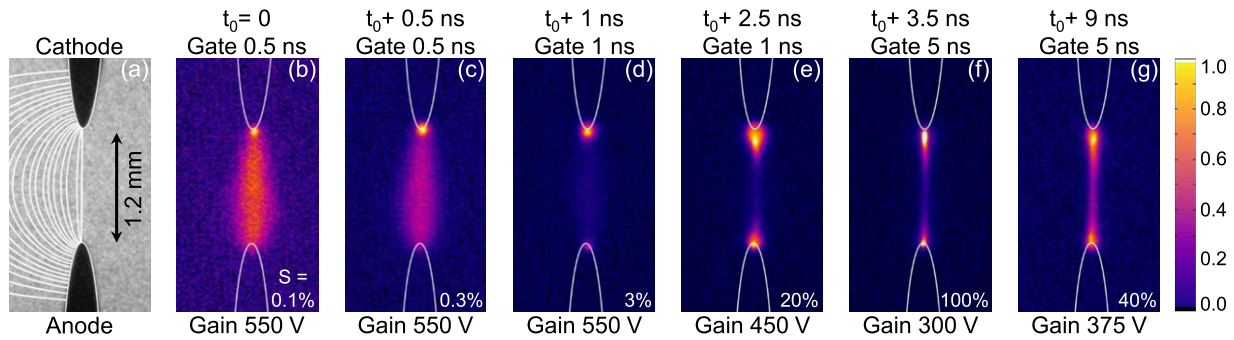


**Figure 4.** Illuminated arrangement showing the electrode shape and position overlaid with calculated electric field lines on the left side (a), discharge emission structures during initial breakdown with 0.5 ns gate (b), (c), and 1 ns gate (d), and during secondary phase with 1 ns gate (e), major emission phase (f) and decay phase (g) with 5 ns gate; the emission starts at  $t_0$  (see figure 5). Each single shot image (i.e. different discharge events) is scaled to maximum intensity and displayed in pseudocolour (note the different iCCD gate widths and gains; the scaling factor  $S$  indicates the percentage of each individual intensity with respect to the overall maximal intensity in (f)).

account (see figure 3), the discharge itself was not modelled in CST; as such, there was no conducting channel in the gap between the electrodes. Consequently, the simulation gives a good approximation of the waveform during the initial slope of the pulse, but it will show deviation from the actual waveform after the rise of the slope, due to the influence of the discharge.

### 3. Results and discussion

Due to the relatively short gap width, the low pulse-repetition frequency, and the high applied HV amplitude, the discharges produced by the setup described above were expected to be in the spark regime, in accordance with the discharge regime maps reported in [16]. However, the spark discharge generated by the HV pulses with sub-ns rise time in this study features two distinct breakdown (or propagation) phases, which could be distinguished as an initial discharge inception during the HV slope, and a subsequent main discharge phase after the HV pulse had reached its maximum. These two discharge phases were investigated by means of iCCD and streak camera recordings. Note that the uncertainty in the synchronisation between the electrical and optical signals has so far failed to reach values below 1 ns, i.e. it cannot be stated precisely at which instant during HV slope the discharge inception occurred.

#### 3.1. Experimental results

Firstly, the 2D discharge emission structure was observed by iCCD single shots with shifted gate positions with respect to the applied HV pulse. The results are displayed in figure 4 for gate widths of 0.5, 1, and 5 ns. The back-illuminated electrodes are shown in figure 4(a), indicating their positions, overlaid with the static electric field lines (i.e. without discharge) calculated by COMSOL Multiphysics<sup>®</sup> using the actual electrode geometry. The initial discharge phase lasts about 1 ns, and features a spot on the cathode tip (at the grounded side at the top), with the discharge emission as an elliptical shape in the volume, with a maximum diameter of  $\approx 400$   $\mu\text{m}$  in the gap centre (see figures 4(b) and (c)). It appears that the envelope of the emission approximately maps the electric field lines around

the gap axis (see figure 4(a)); i.e. there is no spherical inception cloud formation as observed in [24], and no wide ionising front formation as reported in [3, 8] for ns-pulsed discharges. This indicates an immediate breakdown, which is caused by the almost instantly applied high electric field strength across the gap generated by the sub-ns rising HV pulse slope. After the initial phase, the emission becomes stronger around the electrode tips (figure 4(d)), and expands slowly towards the gap centre (figures 4(e) and (f)), a process accompanied by a constriction of the channel to about 100  $\mu\text{m}$  diameter in front of both electrodes. In addition, the emission intensity significantly increases until about 3.5 ns after the first emission. Since the initial phase is much weaker in terms of emission intensity, it had to be recorded with higher multi-channel plate gain, as compared to the main discharge phase. The afterglow starts from  $t_0 + 9$  ns, with a slight increase in the discharge diameter in front of the electrodes. In contrast to the initial breakdown, there is no homogeneous emission over the entire gap during the secondary discharge phase.

For a better understanding of these two phases, streak camera recordings along the discharge channel were subsequently analysed. It is important to note that the streak images only show a 10  $\mu\text{m}$  strip along the axis, i.e. the streak camera slit was positioned exactly on both electrode tips, and only single shots where the discharge directly attached to the electrode tips were accumulated. This could only be achieved by comparing individual discharge events obtained by the simultaneous iCCD and streak camera recordings. The entire discharge development for both phases is shown in figure 5 in a 15 ns window, which can be directly compared to the iCCD images in figure 4. The linearly-scaled streak image (figure 5(a)) clearly indicates that the major part of the emission occurs during the secondary breakdown phase, lasting about 10 ns. Furthermore, the intensity is higher in front of the cathode than in front of the anode. The strong intensity difference between the initial and the secondary breakdown phase is revealed by the logarithmically-scaled image (see figure 5(b)). About 3 ns after the start of the initial phase, there is also a weaker emission in the gap centre, which decays to 10% of the maximum after 40 ns (not shown, measured in a 50 ns time window),

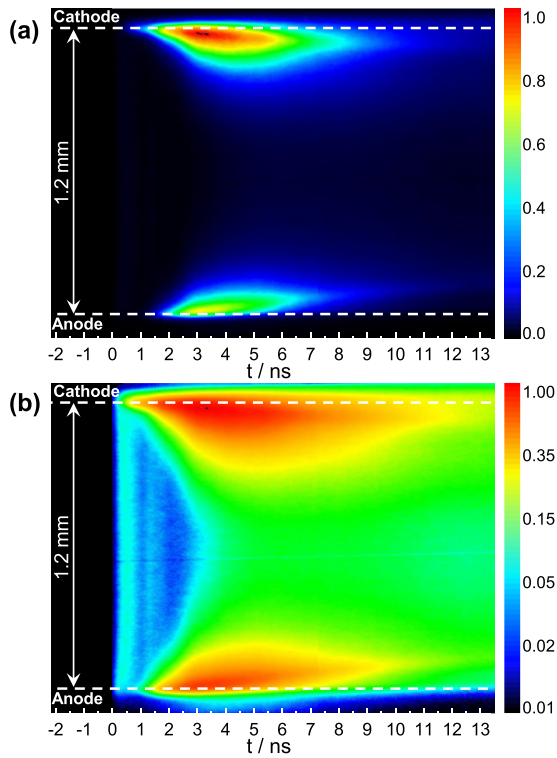


**Figure 5.** Spatio-temporal development of the discharge emission along the gap axis obtained by the streak camera in a 15 ns time window in a linear (a) and a logarithmic (b) intensity scale (accumulation of 100 jitter-corrected streak camera single shots),  $t = 0$  equals  $t_0$  in figure 4.

corresponding to an effective lifetime of the spectrally integrated emission of about 5.6 ns. It should be considered that the radiation and quenching loss processes after the end of the HV pulse are partially compensated by processes leading to a further population of the emitting species in the afterglow. This leads to a relatively long lifetime, as compared to the effective lifetime of  $N_2(C)$  in atmospheric pressure air [25].

Since the initial breakdown phase has to be resolved in order to further analyse the discharge inception, this phase was recorded with the highest resolution in a 0.5 ns window (see figure 6(a)). The discharge emission starts about 20 ps earlier at the cathode than at the anode, and the propagation velocity is much higher from the cathode towards the gap centre, compared to the propagation starting from the anode, as indicated by the white arrows in figure 6(a). The maximal velocity was found in front of the cathode with about  $26 \text{ mm ns}^{-1}$ ; for a cm-sized gap in atmospheric pressure air, similar values were reported for sub-ns rising HV pulses [26]. A slight axial asymmetry is evident, but within about 100 ps, there is significant emission within the entire gap, corresponding to the iCCD image shown in figure 4(b). The analysis of the emission profiles during the initial phase at different gap positions reveals that the emission intensity increases faster in front of the electrodes than in the gap centre (see figure 7(a)). In addition, it is worth noting that the rise of the emission signals in front of both electrodes is about the same as the rise time of the applied HV pulse ( $\approx 200 \text{ ps}$ ), while it is a little slower in the gap centre ( $\approx 300 \text{ ps}$ ).

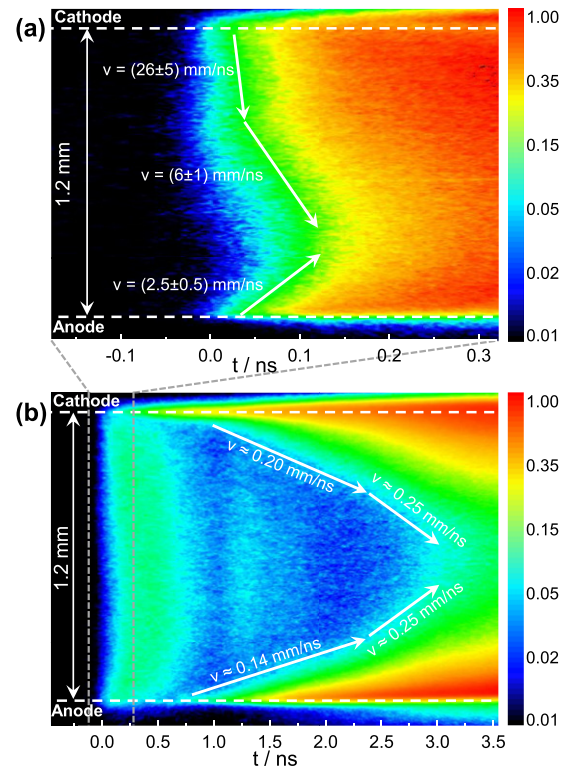


**Figure 6.** Detail of initial and secondary breakdown phase, with indicated propagation velocities in a 0.5 ns window for the initial phase (a) and in a 4 ns window for the secondary phase (b); logarithmical scale with respect to the maximum intensity in each window, i.e. intensities not directly comparable (jitter-corrected accumulation of 300 streak camera single shots).

Just after the end of the initial breakdown phase in the volume, simultaneous (nearly symmetrical) propagations start from the anode and cathode towards the gap centre (see figure 6(b)). These propagations, indicated by white arrows in figure 6(b), are much slower than the ‘regular’ streamer velocities in air ( $\sim 1 \text{ mm ns}^{-1}$ ), which could be an indication of propagation in a highly ionised volume generated by the initial breakdown phase. Similar propagation velocities have been found in single-filament dielectric barrier discharges for high pre-ionisation [7]. However, it is currently unclear whether these propagations are streamers in the classical sense, since the channel formed by the initial phase is usually highly conducting, i.e. there is no need for charge carrier generation by the streamer mechanism. Furthermore, this secondary breakdown phase seems to be similar to the well-known secondary streamer [27], but with different temporal and spatial characteristics.

As shown in figure 6(b), the initial breakdown phase has a duration of about 0.8 ns, which is in accordance with the iCCD recordings. Interestingly, there is a weaker emission in the volume after the end of the initial phase (see figure 6(b)), featuring a slight emission hump from 1.25 to 2.0 ns in the emission profile in the gap centre (see figure 7(b)). This could be related to the dip in the actual applied HV at the electrodes (see figure 2). Moreover, the secondary breakdown phase starts earlier at the cathode, more precisely at the cathode spot (see figure 4(b)), during the initial breakdown phase.

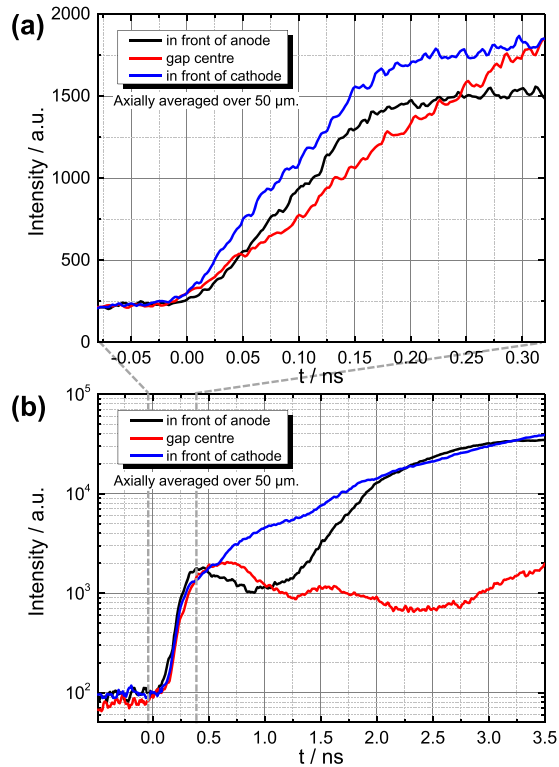


**Figure 7.** Discharge emission profiles at three gap positions for the first emission in linear scale (a), and the complete initial phase in logarithmical intensity scale (b), (extracted from figures 6(a) and (b), respectively).

The delay of about 0.6 ns between the emission occurrences at the cathode and at the anode can be better distinguished in the emission profiles displayed in figure 7(b) (from  $t \approx 0.5$  ns to  $t \approx 1.1$  ns). A possible explanation for this difference could be the accumulation of electrons in front of the anode, leading to a reduction of the electric field strength under the influence of space charges. The excitation of emitting nitrogen molecules by means of electron-neutral collisions requires both a high electron density and high electric field, and is therefore typically predominant in front of the cathode [28]. Furthermore, it is interesting to note that no cathode layer was observed from the streak images, although the spatial resolution is about 2  $\mu\text{m}$ . The most probable reason for the absence of a cathode layer is the continuous production of free electrons due to photoionisation, which plays an important role in air discharges [29].

### 3.2. Numerical modelling of the initial propagation phase

In order to address the issue of which mechanisms are primarily responsible for the fast discharge emission occurrence over the entire gap within about 100 ps, numerical modelling of this initial breakdown phase was conducted. The spatially 2D axisymmetric fluid-Poisson model employed here was adopted from the verified streamer code described in [30] (group name DE). It was extended by including individual balance equations for electrons, negative ions, and the relevant positive ions, in accordance with the reaction kinetic model of Pancheshnyi and Starikovskii [31] for streamer discharges in

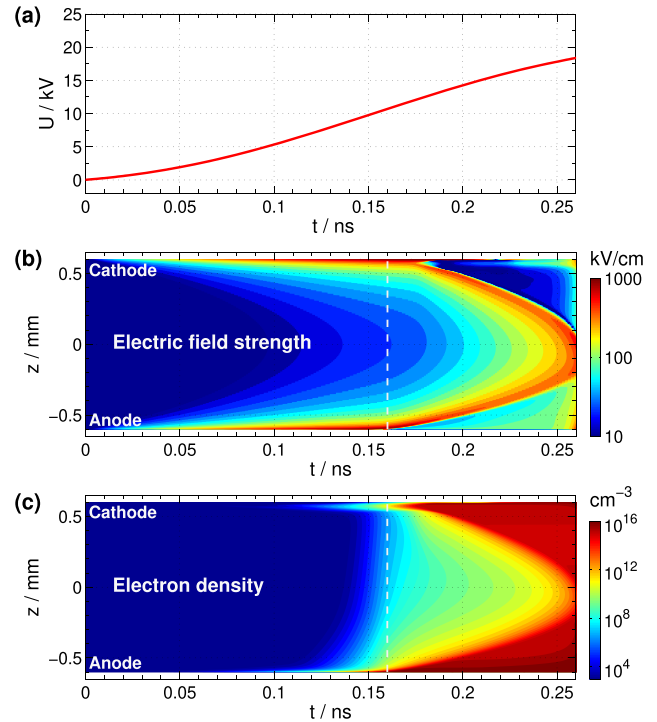


**Figure 8.** Results of the 2D fluid-Poisson model for the initial breakdown phase, using the applied HV pulse (a) obtained by CST simulations as input, for the electric field strength (b) and the electron density (c) in logarithmic scale along the central axis of the gap. The white dashed line indicates the commencement of propagation at  $t = 160$  ps.

air. The local field approximation for the determination of electron transport and rate coefficients was replaced by the local mean energy approximation, in order to prevent the occurrence of erroneous electron transport coefficients at high electric fields, particularly in the gas-electrode interface regions [32]. The HV pulse waveform<sup>5</sup> obtained by CST simulations (see figure 2) and the electrode geometry were used as inputs for the model. Model calculations were carried out using a sub-ps time step, automatically adapted according to physical and numerical requirements. A non-uniform mesh with about 250 000 elements, concentrated in front of the electrode tips, was used to resolve the thin plasma-electrode interface. The modelling results represented in figure 8 show that, with the increase of the applied voltage (see figure 8(a)), a strongly inhomogeneous electric field distribution occurs between the pin electrodes, which is caused by the small curvature of the electrode tips (see figure 8(b)). In the time range from  $t = 0$  to 160 ps, the electric field uniformly increases to values of about  $1000 \text{ kV cm}^{-1}$  at the electrode tips, and  $20 \text{ kV cm}^{-1}$  in the centre of the gap. Until this instant, the electric field is not distorted by space charges. The high electric field strength at both electrode tips leads to a significant increase in the electron density, enabling the almost simultaneous inception of a positive and a negative streamer from the electrode tips (see figure 8(b)).

<sup>5</sup> Note that the instant  $t = 0$  corresponding to the start of the HV pulse (see figure 8(a)) cannot be directly related to the instants of the iCCD and streak camera recordings due to the aforementioned synchronisation uncertainty.

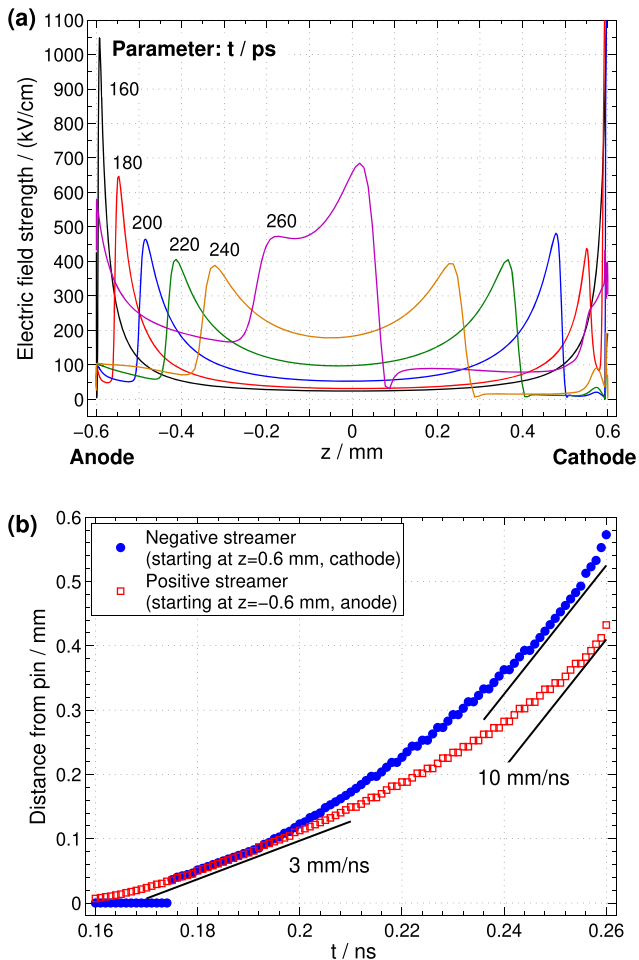


**Figure 9.** Results of the 2D fluid-Poisson model for the electric field strength along the central axis of the gap (a), and the axial distance of the electric field maximum at the streamer head from the respective pin electrode (b) during the initial streamer propagation phase; corresponding velocities are indicated by black solid lines.

Direct electron-collision ionisation of nitrogen molecules is the main electron source at both the cathode and the anode. The moderate increase of the electron density in the volume is caused by photoionisation. The electrons generated here are assumed to be responsible for the excitation of light emitting species during the pre-propagation phase (see figure 6(a)).

The electron density increases in front of both electrodes before the propagations begin (see figure 8(c)), but features a pronounced axial extension of about  $50 \mu\text{m}$  in the volume near the cathode. This can be related to the observed emission occurring first in front of the cathode, since the very first part of the recorded emission during the initial breakdown phase is not a direct measure of the electric field. However, the initiation of the streamers into the volume is instantly visible from the electric field strength calculated by the fluid-Poisson model.

Figure 9(a) shows the electric field strength along the central axis of the gap during the initial streamer propagation phase. Here, it can be seen that at  $t = 160$  ps the electric field is already distorted by the accumulated space charge at the anode side ( $z = -0.6$  mm), and the positive (cathode-directed) streamer propagation is initiated. In contrast, at the cathode side ( $z = 0.6$  mm), the electric field strength is not influenced

by space charges at this instant, reaching a value of about  $1850 \text{ kV cm}^{-1}$  (cut-off in figure 9(a)) at the tip of the electrode pin. Approximately 15 ps later, the negative (anode-directed) streamer starts to form in front of the anode. The deferred start of the negative streamer can be seen more clearly from the spatial position of the maximum electric field in the streamer head, depicted in figure 9(b). This figure shows that the negative streamer bridges a gap of almost 0.6 mm in less than 0.1 ns, while the positive streamer travels about 0.4 mm in 0.1 ns. After a short phase of similar velocities (about  $3 \text{ mm ns}^{-1}$ ), the negative streamer accelerates faster, but finally reaches a similar final velocity to the positive streamer of up to about  $10 \text{ mm ns}^{-1}$ , as indicated in figure 9(b). Due to the faster acceleration of the negative streamer, the counter-propagating streamers do not merge in the centre, but closer to the anode side at about  $t = 260$  ps. Note that the streamer velocities obtained from the fluid-Poisson model are in fair agreement with the propagation velocities deduced from the streak camera images (see figure 6(a)).

Both positive and negative streamers exhibit similar electric field strengths in the streamer head of about 400 to  $700 \text{ kV cm}^{-1}$  (see figure 9(a)). These values are significantly higher than the electric field strength of streamers in air reported elsewhere (about  $200 \text{ kV cm}^{-1}$ , see, e.g. [33, 34]). This could be a consequence of the fast rising applied voltage during streamer propagation enhancing the electric field strength in the streamer head.

In summary, the modelling results indicate the formation of the initial discharge channel by two counter-propagating streamers. Subsequent to the merging of the positive and negative streamers, the ionisation degree within the conducting channel strongly increases, and fast gas heating is likely to occur [35]. Under these circumstances, the validity of the model breaks down, since the corresponding processes have so far not been included. Therefore, the results for later times, showing a high ionisation degree of more than 10% were not analysed further. The inception of glow and spark discharges in air by two counter-propagating streamers was also predicted by computer simulations [36, 37]. However, these simulations reported propagations approximately one order of magnitude slower than those found in the current study, which is likely to be due to their low HV pulse amplitude and 2 ns rise time (leading to lower electric field strengths, especially in combination with longer gaps).

#### 4. Conclusions





The investigation of spark discharges generated by HV pulses with sub-ns rise time revealed a breakdown regime consisting of two phases, both featuring a propagation from the electrodes towards the gap centre, but with different axial and radial characteristics. The combination of fast diagnostics and numerical 2D modelling has provided a greater understanding of the extremely fast discharge inception as two counter-propagation streamers. Experimental and modelling results demonstrate the peculiarity of fast pulsed spark discharges, since the breakdown regime occurring during these steep HV pulses differs significantly from the common streamer breakdown.

However, several open questions arising from these results remain, which should be addressed in future work: e.g. the electrical characterisation of the breakdown phases and the discharge in general, the impact of the gas mixture and electrode geometry, and the extension of the 2D model to reproduce the entire discharge development.

## Acknowledgments

This work was partly supported by the DFG project 408777255. Furthermore, the authors would like to thank S Nijdam (TU/e), M Kettlitz, M Baeva and D Loffhagen (all INP) for fruitful and inspiring discussions, U Nehmzow (glass-blower, INP), the mechanical workshop of the INP for manufacturing the discharge cell, and especially T Franzl and U Denzer (HAMAMATSU Photonics Germany) for their generous supply of the streak camera system.

## ORCID iDs

H Höft  <https://orcid.org/0000-0002-9224-4103>  
 M M Becker  <https://orcid.org/0000-0001-9324-3236>  
 J F Kolb  <https://orcid.org/0000-0002-0434-5001>  
 T Huiskamp  <https://orcid.org/0000-0002-8450-2600>

## References

- [1] Naidis G V, Tarasenko V F, Babaeva N Y and Lomaev M I 2018 *Plasma Sources Sci. Technol.* **27** 013001
- [2] Stepanyan S, Minesi N, Tibère-Inglesse A, Salmon A, Stancu G D and Laux CO 2019 *J. Phys. D: Appl. Phys.* **52** 295203
- [3] Sorokin D A, Tarasenko V F, Beloplotov D V and Lomaev M I 2019 *J. Appl. Phys.* **125** 143301
- [4] Kim H-H 2004 *Plasma Processes Polym.* **1** 91–110
- [5] van Heesch E J M, Winands G J J and Pemen A J M 2008 *J. Phys. D: Appl. Phys.* **41** 234015
- [6] Ono R, Nakagawa Y and Oda T 2011 *J. Phys. D: Appl. Phys.* **44** 485201
- [7] Höft H, Kettlitz M, Becker M M, Hoder T, Loffhagen D, Brandenburg R and Weltmann K-D 2014 *J. Phys. D: Appl. Phys.* **47** 465206
- [8] Tardiveau P, Magne L, Marode E, Ouaras K, Jeanney P and Bournonville B 2016 *Plasma Sources Sci. Technol.* **25** 054005
- [9] Huiskamp T, Hoeben W F L M, Beckers F J C M, van Heesch E J M and Pemen A J M 2017 *J. Phys. D: Appl. Phys.* **50** 405201
- [10] Tardiveau P, Moreau N, Bentaleb S, Postel C and Pasquiers S 2009 *J. Phys. D: Appl. Phys.* **42** 175202
- [11] Tarasenko V F, Naidis G V, Beloplotov D V, Kostyrya I D and Babaeva N Y 2018 *Plasma Phys. Rep.* **44** 746–53
- [12] Babaeva N Y and Naidis G V 2016 *IEEE Trans. Plasma Sci.* **44** 899–902
- [13] Shao T, Zhang C, Niu Z, Yan P, Tarasenko V F, Baksht E K, Burachenko A G and Shut'ko Y V 2011 *Appl. Phys. Lett.* **98** 021503
- [14] Tarasenko V F, Baksht E K, Beloplotov D V, Burachenko A G, Sorokin D A and Lomaev M I 2018 *J. Phys. D: Appl. Phys.* **51** 424001
- [15] Kobayashi S, Bonaventura Z, Tholin F, Popov N A and Bourdon A 2017 *Plasma Sources Sci. Technol.* **26** 075004
- [16] Pai D Z, Lacoste D A and Laux C O 2010 *J. Appl. Phys.* **107** 093303
- [17] Briels T M P, Kos J, Winands G J J, Veldhuizen E M V and Ebert U 2008 *J. Phys. D: Appl. Phys.* **41** 234004
- [18] Komuro A, Ono R and Oda T 2013 *Plasma Sources Sci. Technol.* **22** 045002
- [19] Kettlitz M, Höft H, Hoder T, Reuter S, Weltmann K-D and Brandenburg R 2012 *J. Phys. D: Appl. Phys.* **45** 245201
- [20] Huiskamp T, Beckers F J C M, Hoeben W F L M, van Heesch E J M and Pemen A J M 2016 *Plasma Sources Sci. Technol.* **25** 054006
- [21] Huiskamp T, van Heesch E J M and Pemen A J M 2015 *IEEE Trans. Plasma Sci.* **43** 444–51
- [22] Huiskamp T, Beckers F J C M, van Heesch E J M and Pemen A J M 2016 *IEEE Sens. J.* **16** 3792–801
- [23] Huiskamp T, Beckers F J C M, van Heesch E J M and Pemen A J M 2014 *IEEE Trans. Plasma Sci.* **42** 859–67
- [24] Chen S, Heijmans L C J, Zeng R, Nijdam S and Ebert U 2015 *J. Phys. D: Appl. Phys.* **48** 175201
- [25] Kozlov K V, Brandenburg R, Wagner H-E, Morozov A M and Michel P 2005 *J. Phys. D: Appl. Phys.* **38** 518–29
- [26] Yatom S, Vekselman V, Gleizer J Z and Krasik Y E 2011 *J. Appl. Phys.* **109** 073312
- [27] Marode E 1975 *J. Appl. Phys.* **46** 2005–15
- [28] Raizer Y P 1997 *Gas Discharge Physics* (Berlin: Springer)
- [29] Dubinova A, Teunissen J and Ebert U 2014 *IEEE Trans. Plasma Sci.* **42** 2392–3
- [30] Bagheri B et al 2018 *Plasma Sources Sci. Technol.* **27** 095002
- [31] Pancheshnyi S V and Starikovskii A Y 2003 *J. Phys. D: Appl. Phys.* **36** 2683–91
- [32] Grubert G K, Becker M M and Loffhagen D 2009 *Phys. Rev. E* **80** 036405
- [33] Kulikovskiy A A 1997 *J. Phys. D: Appl. Phys.* **30** 441–50
- [34] Babaeva N Y and Naidis G V 1996 *J. Phys. D: Appl. Phys.* **29** 2423–31
- [35] Popov N A 2011 *J. Phys. D: Appl. Phys.* **44** 285201
- [36] Tholin F and Bourdon A 2011 *J. Phys. D: Appl. Phys.* **44** 385203
- [37] Tholin F and Bourdon A 2013 *J. Phys. D: Appl. Phys.* **46** 365205